Application of Surface Spline Interpolation in Inversion of Bottom Friction Coefficients

ZHENG GUO AND HAIDONG PAN

Physical Oceanography Laboratory, Qingdao Collaborative Innovation Center of Marine Science and Technology (CIMST), Ocean University of China, and Qingdao National Laboratory for Marine Science and Technology, Qingdao, China

WEI FAN

Ocean College, Zhejiang University, Zhoushan, China

XIANQING LV

Physical Oceanography Laboratory, Qingdao Collaborative Innovation Center of Marine Science and Technology (CIMST), Ocean University of China, and Qingdao National Laboratory for Marine Science and Technology, Qingdao, China

(Manuscript received 10 January 2017, in final form 28 June 2017)

ABSTRACT

A new method for the inversion of bottom friction coefficients (BFCs) in a two-dimensional tidal model is proposed in this study. In this method, the field of BFCs is constructed by interpolating values at independent points using a surface spline. The surface spline interpolation has an advantage: that the constructed surface is smoother than the surface constructed by the traditionally used linear interpolation, which has unrealistic extrema. The method is validated in twin experiments where the prescribed nonlinear distribution of BFCs are better inverted with the surface spline interpolation. In practical experiments, the BFCs are inverted and the M_2 tide in the Bohai Sea is simulated by assimilating the TOPEX/Poseidon (T/P) data. The small errors between the simulation results and the observations, as well as the accurate cotidal charts, demonstrate the feasibility of the new method in practical application.

1. Introduction

As important motion forms of ocean water, tidally induced currents are an area of interest to researchers. Bottom friction plays an important role in the tidal phenomenon. Therefore, accurate estimation of bottom friction contributes to successful tide modeling. Many schemes of parameterization have been proposed for the bottom friction, of which the "quadratic friction" is widely used (Tierney et al. 2000; Egbert and Ray 2000; Moe et al. 2002). In this scheme, the bottom friction F is defined using a quadratic drag law through the coefficient k:

$$F = -k\frac{|\mathbf{u}|}{H}\mathbf{u}. \tag{1}$$

The bottom friction coefficient (BFC) k is usually set either as a constant or is used as a function of depth (Kang et al. 1998; Lee et al. 2002; Egbert et al. 2004; Sannino et al. 2004). But a more efficient and accurate way to estimate the BFC is through data assimilation using the adjoint method, as demonstrated in Wang et al. (2014).They made a comprehensive comparison of different schemes of BFCs, including a constant for the entire domain, different constants for different subdomains, depth-dependent BFCs, and BFCs inverted with the adjoint method; and concluded that the best simulation of the M_2 constituent was obtained with BFCs inverted by the adjoint method.

In data assimilation, an optimal initial model state or model parameter can be found to minimize the distance between the model output and observations. As one parameter of particular importance, the BFC has been estimated through data assimilation in many studies (Das and Lardner 1991, 1992; Lu and Zhang 2006). Because it is impractical and sometimes impossible to take the BFCs at all grid points as parameters (Ullman and Wilson 1998; Heemink et al. 2002), the independent points scheme is usually adopted, which means that BFCs at some selected points, or independent points, are treated as independent parameters and that values at other points are obtained by interpolation. This scheme reduces the number of control variables, serving as a

Corresponding author: Wei Fan, fanwei@zju.edu.cn; Xianqing Lv, xqinglv@ouc.edu.cn

DOI: 10.1175/JTECH-D-17-0012.1

great solution for the ill-posedness of the inversion problem (Zhang and Wang 2014).

Thus what remains to be dealt with is interpolation. The BFC field obtained by interpolation can be expressed as

$$k_{i,j} = \sum_{l=1}^{N} W_{i,j}^{l} k_l, \tag{2}$$

where $k_{i,j}$ is the BFC at the grid point (i,j), k_l is the lth independent BFC, and $W_{i,j}^{l}$ is the coefficient of interpolation. Traditionally, linear interpolation is used and the coefficient is calculated by (Lu and Zhang 2006)

$$W_{i,j}^{l} = \frac{w_{i,j}^{l}}{\sum_{l=1}^{N} w_{i,j}^{l}}, \tag{3}$$

where $w_{i,j}^{l} = \dfrac{R^2 - (r_{i,j}^{l})^2}{R^2 + (r_{i,j}^{l})^2}$ is the Cressman weight, $r_{i,j}^{l}$ is the distance between the grid point (i,j) and the lth independent point, and R is the influence radius set based on experience. Although the interpolation with the Cressman weight (CI) yields satisfying results in general (Lu and Zhang 2006), the reconstructed BFC field is unsmooth, sometimes showing unrealistic bull's-eye patterns around the independent points. This motivates us to seek a more reasonable interpolation method to combine with the adjoint method. As one popular technique for data interpolation, the surface spline (also known as thin plate spline) has the advantage, among others, of producing smooth surfaces. It was first proposed by Harder and Desmarais (1972) for interpolating wing deflections and computing slopes for aeroelastic calculations. The surface spline and its variations have been applied successfully in oceanographic and meteorological contexts (Brankart and Brasseur 1996; Luo et al. 2008), where the spatial distribution of many parameters is smooth surface. Based on its proven great performance, the surface spline interpolation (SSI) is applied to the inversion of BFCs with an adjoint tidal model in this study.

The paper is organized as follows. The numerical model and the implementation of SSI in the model is introduced in section 2. Twin experiments and practical experiments are conducted in section 3 to assess the performance of SSI in the inversion of BFCs. The summary in section 4 completes the paper.

2. Numerical model and settings

a. Forward model

The governing equations of the depth-averaged two-dimensional tidal model are as follows:

$$\begin{aligned}
&\frac{\partial \zeta}{\partial t} + \frac{\partial[(h+\zeta)u]}{\partial x} + \frac{\partial[(h+\zeta)v]}{\partial y} = 0\\
&\frac{\partial u}{\partial t} + u\frac{\partial u}{\partial x} + v\frac{\partial u}{\partial y} - fv + \frac{ku\sqrt{u^2+v^2}}{h+\zeta}\\
&\quad - A\left(\frac{\partial^2 u}{\partial x^2} + \frac{\partial^2 u}{\partial y^2}\right) + g\frac{\partial \zeta}{\partial x} = 0\\
&\frac{\partial v}{\partial t} + u\frac{\partial v}{\partial x} + v\frac{\partial v}{\partial y} + fu + \frac{kv\sqrt{u^2+v^2}}{h+\zeta}\\
&\quad - A\left(\frac{\partial^2 v}{\partial x^2} + \frac{\partial^2 v}{\partial y^2}\right) + g\frac{\partial \zeta}{\partial v} = 0,
\end{aligned} \tag{4}$$

where t is time; h is the undisturbed sea level; ζ is the sea surface elevation above h; u and v are zonal and meridional velocity, respectively; f is the Coriolis parameter; g is the acceleration as a result of gravity; A is the horizontal eddy viscosity coefficient; and k is the BFC to be estimated in this study.

b. Adjoint model

The adjoint model is used to optimize BFCs to minimize the distance between the model output and observations. The distance is expressed as the cost function J:

$$J = \frac{1}{2} K_\zeta \int_\Sigma (\zeta - \hat{\zeta})^2 d\sigma, \tag{5}$$

where K_ζ is a constant, Σ is the set of observation locations, and $\hat{\zeta}$ is the observed surface elevation. The Lagrangian function is defined as

$$\begin{aligned}
L(\zeta,u,v,\lambda,\mu,\nu,k) = J(\zeta) + \int_\Sigma &\lambda\left\{\frac{\partial \zeta}{\partial t} + \frac{\partial[(h+\zeta)u]}{\partial x} + \frac{\partial[(h+\zeta)v]}{\partial y}\right\}\\
&+ \mu\left\{\frac{\partial u}{\partial t} + u\frac{\partial u}{\partial x} + v\frac{\partial u}{\partial y} - fv + \frac{ku\sqrt{u^2+v^2}}{h+\zeta} - A\left(\frac{\partial^2 u}{\partial x^2} + \frac{\partial^2 u}{\partial y^2}\right) + g\frac{\partial \zeta}{\partial x}\right\}\\
&+ \nu\left\{\frac{\partial v}{\partial t} + u\frac{\partial v}{\partial x} + v\frac{\partial v}{\partial y} + fu + \frac{kv\sqrt{u^2+v^2}}{h+\zeta} - A\left(\frac{\partial^2 v}{\partial x^2} + \frac{\partial^2 v}{\partial y^2}\right) + g\frac{\partial \zeta}{\partial v}\right\} d\sigma,
\end{aligned} \tag{6}$$

where λ, μ, and v are adjoint variables of ζ, u, and v, respectively. According to the typical theory of the Lagrangian multiplier method, the adjoint model can be constructed by the following equations:

$$\frac{\partial L}{\partial \zeta} = 0, \quad \frac{\partial L}{\partial u} = 0, \quad \frac{\partial L}{\partial v} = 0. \tag{7}$$

Equations of the adjoint model are the same with Wang et al. (2014). The numerical scheme of the forward and adjoint equations are similar to Lu and Zhang (2006).

c. *Optimization of independent BFCs*

We look for the optimal model parameters—BFCs at all grid points in this case—to minimize J using the optimization and adjoint methods. According to the typical steepest descent method,

$$k_l^{i+1} = k_l^i + \alpha^i \cdot p_l^i, \tag{8}$$

where i denotes the iteration step, k_l is the lth parameter, α is the step factor that is set as a small positive number in order to ensure that the cost function decreases continuously without fluctuations, and p is the negative of the gradient of J in respect to k_l. It should be noted that in this study, the gradient is scaled, that is,

$$p_l = -\frac{\partial J}{\partial k_l} \Bigg/ \sqrt{\sum_{l=1}^{N} \left(\frac{\partial J}{\partial k_l}\right)^2}, \tag{9}$$

where N is the number of independent parameters. The gradient can be obtained by solving the equation, $\frac{\partial L}{\partial k} = 0$. We arrive at

$$\frac{\partial J}{\partial k} = -\left(\frac{\mu u\sqrt{u^2+v^2}}{h+\zeta} + \frac{vv\sqrt{u^2+v^2}}{h+\zeta}\right). \tag{10}$$

If we select BFCs at some grid points as independent parameters and construct the whole BFC field using Eq. (2), the gradient of the cost function, now denoted by $\hat{J}$, with respect to the lth independent BFC is

$$\frac{\partial \hat{J}}{\partial k_l} = \frac{\partial J}{\partial k_l} + \sum_{i,j} W_{i,j}^l \frac{\partial J}{\partial k_{i,j}}, \tag{11}$$

where (i,j) denotes grid points within the influence radius of the lth independent BFC.

When CI is adopted, the coefficient of interpolation W is calculated according to Eq. (3). In this study, we combine SSI with the adjoint method and the SSI coefficients are derived as follows.

Assuming that BFCs are known at N points, the whole BFC field can be constructed with a variation of the surface spline. The BFC at grid points (i,j) is expressed as (Liu et al. 2002)

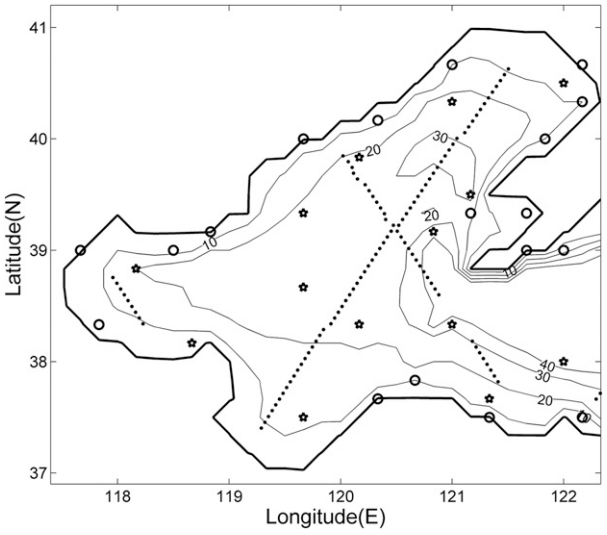

FIG. 1. Bathymetry of the Bohai Sea (m), position of the T/P satellite tracks (dots), and tidal gauge stations (circles), as well as the distribution of independent points (stars).

$$k_{i,j} = \sum_{l=1}^{N} A_l \left(\frac{r_{ij,l}^2}{R^2} \ln \frac{r_{ij,l}^2}{R^2} + 1 - \frac{r_{ij,l}^2}{R^2}\right), \tag{12}$$

where $r_{ij,l}$ is the distance between point (i,j) and the lth independent point, R is a prescribed radius, and A_k is the coefficient to be determined. Based on Eq. (12), the relationship between one known BFC and the others is expressed in matrix form as

$$\mathbf{XA} = \mathbf{B} \tag{13}$$

The detailed forms of the three matrixes are given as

$$\mathbf{A} = (A_i)_{N\times 1},$$
$$\mathbf{B} = (k_i)_{N\times 1},$$
$$\mathbf{X} = (w_{ij})_{N\times N},$$

where

$$w_{ij} = \begin{cases} 1, & i = j \\ \dfrac{r_{ij}^2}{R^2} \ln \dfrac{r_{ij}^2}{R^2} + 1 - \dfrac{r_{ij}^2}{R^2}, & i \neq j \end{cases}$$

and r_{ij} is the distance between the ith and jth independent points. If we set $\mathbf{C} = \mathbf{X}^{-1}$, then Eq. (13) can be changed into $\mathbf{A} = \mathbf{CB}$. Then we get

$$A_k = \sum_{l=1}^{N} C_{k,l} k_l. \tag{14}$$

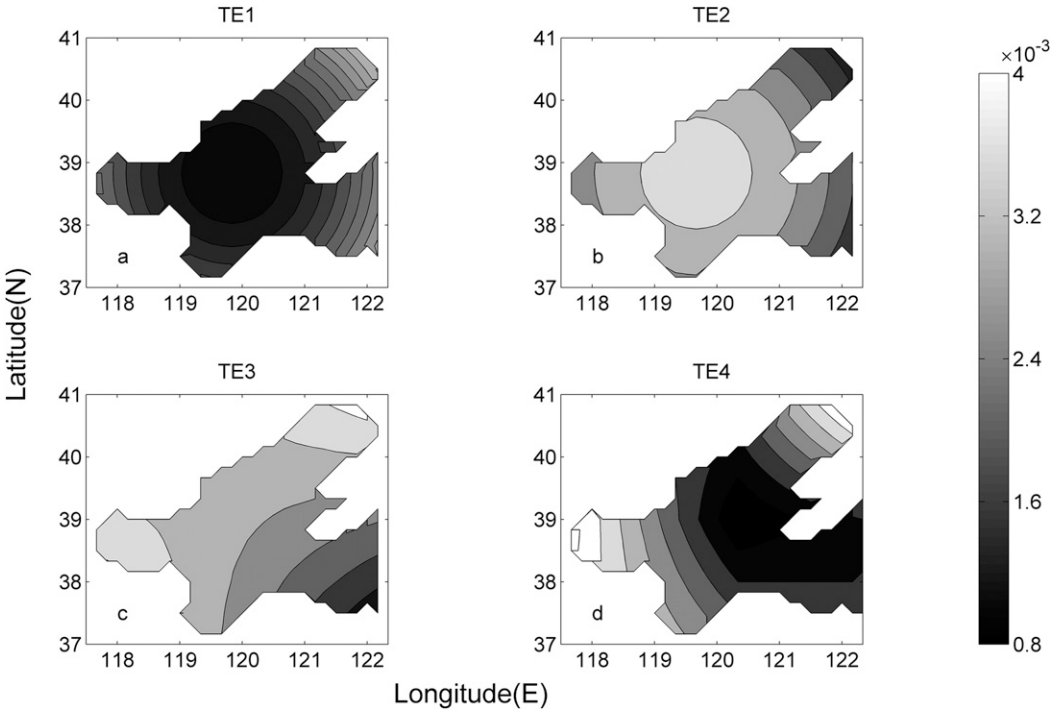

FIG. 2. Four prescribed BFC fields in TEs: (a) a paraboloid opening upward (TE1), (b) a paraboloid opening downward (TE2), (c) a bilinear surface (TE3), and (d) a surface composed of 4 bilinear patches (TE4).

Plug Eq. (14) into Eq. (12) and we arrive at

$$k_{i,j} = \sum_{m=1}^{N}\sum_{l=1}^{N} C_{m,l}k_l\left(\frac{r_{ij,m}^2}{R^2}\ln\frac{r_{ij,m}^2}{R^2} + 1 - \frac{r_{ij,m}^2}{R^2}\right). \quad (15)$$

By interchanging the order of the summation, Eq. (15) is rewritten into the form of Eq. (2):

$$k_{i,j} = \sum_{l=1}^{N} W_{i,j}^l k_l,$$

where $W_{i,j}^l = \sum_{m=1}^{N} C_{m,l}\left(\frac{r_{ij,m}^2}{R^2}\ln\frac{r_{ij,m}^2}{R^2} + 1 - \frac{r_{ij,m}^2}{R^2}\right)$ is the coefficient corresponding to the lth independent BFC at the point (i,j).

d. *Independent points scheme*

The independent points are selected based on the gradient of the water depth. The basic idea is that as the bottom friction is closely related to water depth, more independent points will be needed to depict the distribution of BFCs if the water depth varies greatly or has a large gradient. Details on how to select independent points can be found in Lu and Zhang (2006). In this study, 14 independent points are selected and shown in Fig. 1.

e. *Settings*

The model adopts the Arakawa C grid. The area of computation is the Bohai Sea, covering 37°–41°N, 117.5°–122.5°E with a space resolution of 1/6° × 1/6°. As

TABLE 1. Statistical analysis of the amplitude and phase of the M_2 tide, as well as the BFCs in four TEs. Skill is the model skill defined in Eq. (18), RMS (10^{-4}) is the root-mean-square error, and E (%) is the relative average error.

		TE1		TE2		TE3		TE4	
		SSI	CI	SSI	CI	SSI	CI	SSI	CI
Amplitude	Skill	1.00	1.00	0.99	0.99	1.00	1.00	0.99	1.00
Phase	Skill	1.00	1.00	1.00	1.00	1.00	1.00	1.00	1.00
BFC	Skill	0.97	0.93	0.95	0.92	0.92	0.96	0.95	0.97
	RMS	1.86	2.53	2.62	2.83	2.87	2.14	3.95	3.52
	E	6.65	12.77	10.44	13.48	13.53	7.34	8.05	6.09

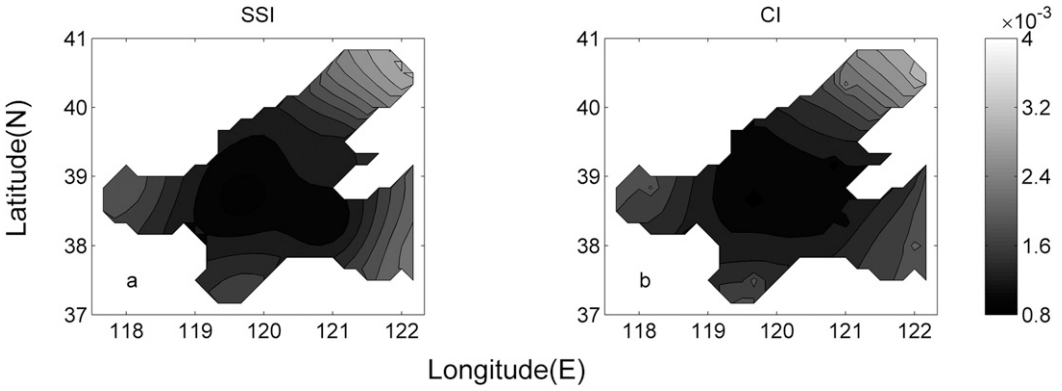

FIG. 3. BFC fields inverted by the adjoint model combined with (a) SSI and (b) CI in TE1, in which the BFC field is prescribed as a paraboloid opening upward.

we focus on the development of the method, only the M_2 tide is simulated. Therefore, the time step is 1/120 of the period of the M_2 tide. The bathymetry of the Bohai Sea, the positions of tidal gauge stations, and TOPEX/Poseidon (T/P) satellite tracks in this area are shown in Fig. 1.

3. Numerical experiments

a. Twin experiments

Twin experiments (TEs) are conducted to evaluate the feasibility of SSI in inversion of BFCs. In TEs, harmonic constants of the M_2 tide along the T/P tracks and at tidal gauge stations are obtained by the forward model that is run with a prescribed BFC field. These data are regarded as "observations." Then run the forward model with an initial guess of BFCs and the difference between the simulated results and the observations along the T/P tracks serves as the external force for the adjoint model. Thereafter, run the adjoint model. With variables obtained from the forward and adjoint models, BFCs are optimized according to Eq. (8). Repeat the procedure with BFCs being optimized until certain criteria are met.

The performance of SSI or CI in combination with the adjoint model is evaluated by the following statistics (Zhong et al. 2010): the root-mean-square (RMS) error

$$\mathrm{RMS} = \sqrt{\frac{1}{N}\sum_{i=1}^{N}(x_{\mathrm{mod}} - x_{\mathrm{obs}})^2}. \tag{16}$$

The relative average error E computed according to

$$E = \frac{\sum_{i=1}^{N}(x_{\mathrm{mod}} - x_{\mathrm{obs}})^2}{\sum_{i=1}^{N}(|x_{\mathrm{mod}} - \bar{x}_{\mathrm{obs}}|^2 + |x_{\mathrm{obs}} - \bar{x}_{\mathrm{obs}}|^2)}, \tag{17}$$

where x is the tidal amplitude or phase, or BFC in the twin experiments because the "true" BFC field is known; $\bar{x}$ is the average over space; and subscripts "mod" and "obs" denote the model results and observations at the tidal

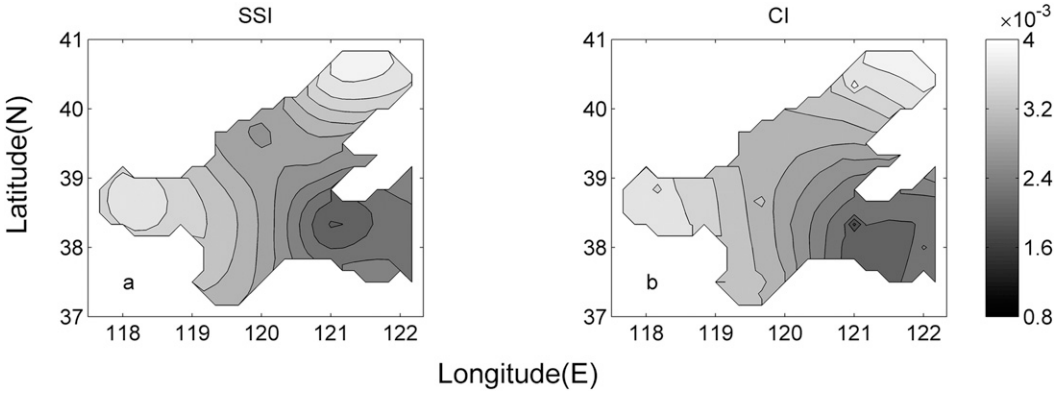

FIG. 4. As in Fig. 3, but for TE3 in which the BFC field is prescribed as a bilinear surface.

TABLE 2. Statistical analysis of the amplitude and phase of the M_2 tide.

	Amplitude			Phase		
	Skill	RMS	E	Skill	RMS	E
SSI	0.99	7.24	2.88	1.00	5.93	0.14
CI	0.99	7.26	2.89	1.00	5.71	0.13

gauge stations, respectively. Following Warner et al. (2005), we also compute the model skill according to

$$\text{skill} = 1 - \frac{\sum_{i=1}^{N} (x_{\text{mod}} - x_{\text{obs}})^2}{\sum_{i=1}^{N} (|x_{\text{mod}} - \bar{x}_{\text{obs}}| + |x_{\text{obs}} - \bar{x}_{\text{obs}}|)^2}. \quad (18)$$

Perfect agreement between the model results and the observations yields a skill of 1, while complete disagreement yields 0.

In TEs, four BFC fields are prescribed (Fig. 2): a paraboloid opening upward (TE1), a paraboloid opening downward (TE2), a bilinear surface (TE3), and a surface composed of four bilinear patches (TE4).

The results of the four TEs are summarized in Table 1. The model skill in terms of the amplitude and phase of the M_2 tide is 0.99 or 1 in all experiments, demonstrating the successful simulation of sea surface elevation. Therefore, we focus on the inversion of BFCs to compare the two interpolation methods.

In TE1, the skill of the model combined with SSI to invert BFCs is 0.97, showing a slight advantage over that with CI, which is 0.93. The advantage is also embodied in a smaller root-mean-square error and relative average error. Figure 3 shows that BFC fields inverted by the adjoint model combined with both methods are consistent with the prescribed field. However, the CI results display a bull's-eye pattern, which is a common problem caused by the interpolation method. An analysis of the TE2 results lead to the same conclusions: In TE3 and TE4, CI outperforms SSI by a little, demonstrated by the model skill, the root-mean-square error, and the relative average error shown in Table 1. However, the bull's-eye pattern still exists in the results obtained with CI (Fig. 4).

b. *Practical experiments*

Performance of the adjoint model combined with the two methods is also evaluated in a practical context. Harmonic constants of the M_2 constituent extracted from T/P along-track data (from October 1992 to July 2002) are assimilated into the model. Tidal gauge data are used for evaluation of the simulated results. Statistical results are shown in Table 2, which demonstrates that the tidal simulation is successful with both interpolation methods. This statement is further confirmed by cotidal charts of the M_2 constituent (Fig. 5), which show the accurate location of amphidromic points near Qinghuangdao and the Yellow River delta. The inverted BFC fields are shown in Fig. 6. On the whole the cotidal charts show similar patterns, that BFCs are larger in Laizhou Bay, Bohai Bay, and Liaodong Bay, while BFCs are smaller in deeper water. However, on closer inspection the BFC surface obtained with SSI is found to be smoother, while that obtained with CI has bumps and depressions around several independent points.

c. *Discussion*

BFCs are introduced for parameterization of the bottom friction. However, the real BFC field is difficult to measure directly for evaluation of inversion results.

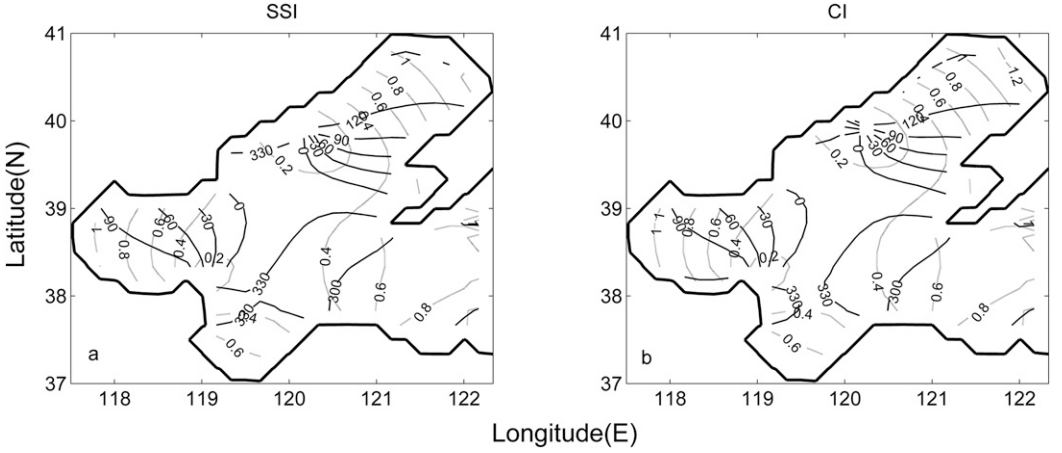

FIG. 5. Cotidal charts for the M_2 constituent in the Bohai Sea obtained with the adjoint model combined with (a) SSI and (b) CI. Shown are coamplitude lines (m, dashed lines) and cophase lines (°, solid lines).

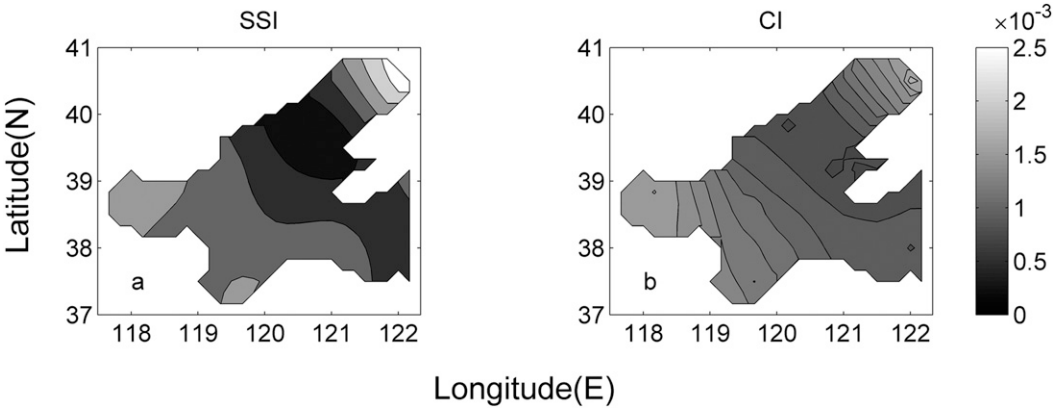

FIG. 6. BFC fields inverted with the adjoit method combined with (a) SSI and (b) CI.

Here arises the problem of choosing a more appropriate interpolation method to obtain a BFC field closer to the real one.

A phenomenon found in the abovementioned experiments is that the CI results usually show unrealistic extrema around independent points. Although we would like to reduce the number of independent parameters while capturing features of the BFCs field (Lu and Zhang 2006; Zhang and Wang 2014), the distribution of independent points selected according to water depth is irregular. To ensure that BFCs at any grid point can be obtained by interpolation, the CI influence radius should be larger than a certain value. Consequently, the bull's-eye pattern, especially around dense independent points, is hard to eliminate. In this respect, SSI is more appropriate for the inversion of BFCs.

Although the real BFCs are difficult to measure directly, previous studies show that they are associated with water depth and bottom roughness (Mofjeld 1988; Ullman and Wilson 1998; Li et al. 2004). The fact is obvious that the distribution of water depth and bottom roughness in the Bohai Sea (Li et al. 2014) is nonlinear along any direction. Thus, the real distribution of BFCs, as a function of water depth, bottom roughness, and other parameters, is more likely to be a nonlinear surface. Twin experiments demonstrate that the adjoint model combined with SSI performs better in the inversion of nonlinear surfaces (TE1 and TE2), while that combined with CI performs better in the inversion of bilinear surfaces (TE3 and TE4). This is confirmed by interpolating the bathymetry of the Bohai Sea. We use the same independent points as in previous experiments to reconstruct the bathymetry of the Bohai Sea by the two interpolation methods. Figure 7 shows that the bathymetry interpolated with the surface spline is closer to the real one. The skills of SSI and CI are 0.89 and 0.83, respectively, indicating the superiority of SSI. Therefore, we believe that the BFC field inverted by the model combined with SSI is closer to the real field.

4. Summary

The adjoint method is an efficient way to determine BFCs, but too many control variables often lead to

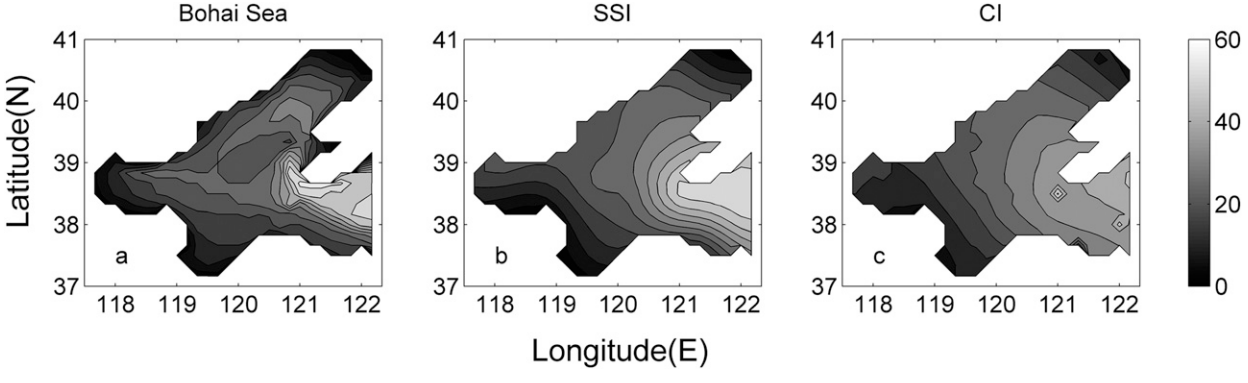

FIG. 7. (a) Bathymetry of the Bohai Sea (m) and those obtained with (b) SSI and (c) CI.

ill-posedness of the inverse problem. The independent points strategy serves as a satisfactory solution, where the BFC field is constructed by interpolating the values of a group of independent points under the assumption of spatially varying BFCs. This study explores the feasibility of SSI as an alternative to the traditionally used linear interpolation. The adjoint model combined with SSI is evaluated in the simulation of the M_2 tide in the Bohai Sea by optimizing the BFCs. In twin experiments, SSI outperforms CI in the inversion of the nonlinear distribution of BFCs. In addition, the surface of BFCs reconstructed by SSI is smoother, while BFCs reconstructed by CI has unexpected extrema. In practical experiments, the BFCs are optimized and the M_2 tide is simulated by assimilating T/P data. The accurate cotidal charts indicate the feasibility of SSI in the inversion of BFC in practical application.

Acknowledgments. This research was supported by the National Natural Science Foundation of China through Grant 41606006, the National Key Research and Development Plan through Grant 2016YFC1402304, the Key Research and Development Plan of Shandong Province through Grant 2016ZDJS09A02, the National Natural Science Foundation of China through Grant 41506015, and the Natural Science Foundation of Zhejiang Province through Grant LY16D060001.

REFERENCES

Brankart, J.-M., and P. Brasseur, 1996: Optimal analysis of in situ data in the western Mediterranean using statistics and cross-validation. *J. Atmos. Oceanic Technol.*, **13**, 477–491, doi:10.1175/1520-0426(1996)013<0477:OAOISD>2.0.CO;2.

Das, S., and R. Lardner, 1991: On the estimation of parameters of hydraulic models by assimilation of periodic tidal data. *J. Geophys. Res.*, **96**, 15 187–15 196, doi:10.1029/91JC01318.

——, and ——, 1992: Variational parameter estimation for a two-dimensional numerical tidal model. *Int. J. Numer. Methods Fluids*, **15**, 313–327, doi:10.1002/fld.1650150305.

Egbert, G. D., and R. D. Ray, 2000: Significant tidal dissipation in the deep ocean inferred from satellite altimeter data. *Nature*, **405**, 775–778, doi:10.1038/35015531.

——, ——, and B. G. Bills, 2004: Numerical modeling of the global semidiurnal tide in the present day and in the last glacial maximum. *J. Geophys. Res.*, **109**, C03003, doi:10.1029/2003JC001973.

Harder, R. L., and R. N. Desmarais, 1972: Interpolation using surface splines. *J. Aircr.*, **9**, 189–191, doi:10.2514/3.44330.

Heemink, A. W., E. E. A. Mouthaan, M. R. T. Roest, E. A. H. Vollebregt, K. B. Robaczewska, and M. Verlaan, 2002: Inverse 3D shallow water flow modelling of the continental shelf. *Cont. Shelf Res.*, **22**, 465–484, doi:10.1016/S0278-4343(01)00071-1.

Kang, S. K., S.-R. Lee, and H.-J. Lie, 1998: Fine grid tidal modeling of the Yellow and East China Seas. *Cont. Shelf Res.*, **18**, 739–772, doi:10.1016/S0278-4343(98)00014-4.

Lee, H. J., K. T. Jung, J. K. So, and J. Y. Chung, 2002: A three-dimensional mixed finite-difference Galerkin function model for the oceanic circulation in the Yellow Sea and the East China Sea in the presence of M_2 tide. *Cont. Shelf Res.*, **22**, 67–91, doi:10.1016/S0278-4343(01)00068-1.

Li, C., A. Valle-Levinson, L. P. Atkinson, K. C. Wong, and K. M. M. Lwiza, 2004: Estimation of drag coefficient in James River Estuary using tidal velocity data from a vessel-towed ADCP. *J. Geophys. Res.*, **109**, C03034, doi:10.1029/2003JC001991.

Li, G., P. Li, Y. Liu, L. Qiao, Y. Ma, J. Xu, and Z. Yang, 2014: Sedimentary system response to the global sea level change in the East China Seas since the last glacial maximum. *Earth-Sci. Rev.*, **139**, 390–405, doi:10.1016/j.earscirev.2014.09.007.

Liu, D., J. Zhang, and S. Wang, 2002: Constrained fitting of faulted bedding planes for three-dimensional geological modeling. *Adv. Eng. Software*, **33**, 817–824, doi:10.1016/S0965-9978(02)00024-8.

Lu, X., and J. Zhang, 2006: Numerical study on spatially varying bottom friction coefficient of a 2D tidal model with adjoint method. *Cont. Shelf Res.*, **26**, 1905–1923, doi:10.1016/j.csr.2006.06.007.

Luo, W., M. C. Taylor, and S. R. Parker, 2008: A comparison of spatial interpolation methods to estimate continuous wind speed surfaces using irregularly distributed data from England and Wales. *Int. J. Climatol.*, **28**, 947–959, doi:10.1002/joc.1583.

Moe, H., A. Ommundsen, and B. Gjevik, 2002: A high resolution tidal model for the area around the Lofoten Islands, northern Norway. *Cont. Shelf Res.*, **22**, 485–504, doi:10.1016/S0278-4343(01)00078-4.

Mofjeld, H. O., 1988: Depth dependence of bottom stress and quadratic drag coefficient for barotropic pressure-driven currents. *J. Phys. Oceanogr.*, **18**, 1658–1669, doi:10.1175/1520-0485(1988)018<1658:DDOBSA>2.0.CO;2.

Sannino, G., A. Bargagli, and V. Artale, 2004: Numerical modeling of the semidiurnal tidal exchange through the Strait of Gibraltar. *J. Geophys. Res.*, **109**, C05011, doi:10.1029/2003JC002057.

Tierney, C., J. Wahr, F. Bryan, and V. Zlotnicki, 2000: Short-period oceanic circulation: Implications for satellite altimetry. *Geophys. Res. Lett.*, **27**, 1255–1258, doi:10.1029/1999GL010507.

Ullman, D. S., and R. E. Wilson, 1998: Model parameter estimation from data assimilation modelling: Temporal and spatial variability of the bottom drag coefficient. *J. Geophys. Res.*, **103**, 5531–5549, doi:10.1029/97JC03178.

Wang, D., Q. Liu, and X. Lv, 2014: A study on bottom friction coefficient in the Bohai, Yellow, and East China Sea. *Math. Probl. Eng.*, **2014**, 432529, doi:10.1155/2014/432529.

Warner, J. C., W. R. Geyer, and J. A. Lerczak, 2005: Numerical modeling of an estuary: A comprehensive skill assessment. *J. Geophys. Res.*, **110**, C05001, doi:10.1029/2004JC002691.

Zhang, J., and Y. P. Wang, 2014: A method for inversion of periodic open boundary conditions in two-dimensional tidal models. *Comput. Methods Appl. Mech. Eng.*, **275**, 20–38, doi:10.1016/j.cma.2014.02.020.

Zhong, L., M. Li, and D.-L. Zhang, 2010: How do uncertainties in hurricane model forecasts affect storm surge predictions in a semi-enclosed bay? *Estuarine Coastal Shelf Sci.*, **90**, 61–72, doi:10.1016/j.ecss.2010.07.001.